Curved fluid membranes behave laterally as an effective viscoelastic medium

Mohammad Rahimi,[a], Antonio DeSimone,[b] and Marino Arroyo,[a*]

The lateral mobility of membrane inclusions is essential in biological processes involving membrane-bound macromolecules, which often take place in highly curved geometries such as membrane tubes or small organelles. Probe mobility is assisted by lateral fluidity, which is thought to be purely viscous for lipid bilayers and synthetic systems such as polymersomes. In previous theoretical studies, the hydrodynamical mobility is estimated assuming fixed membrane geometry. However, fluid membranes are very flexible out-of-plane. By accounting for the deformability of the membrane and in the presence of curvature, we show that the lateral motion of an inclusion produces a normal force, which results in a nonuniform membrane deformation. Such a deformation mobilizes bending elasticity, produces extra lateral viscous and elastic forces, and results in an effective lateral viscoelastic behavior. The coupling between lateral and out-of-plane mechanics is mediated by the interfacial hydrodynamics and curvature. We analyze the frequency and curvature dependent rheology of flexible fluid membranes, and interpret it with a simple four-element model, which provides a background for microrheological experiments. Two key technical aspects of the present work are a new formulation for the interfacial hydrodynamics, and the linearization of the governing equations around a cylindrical geometry.

1 Introduction

Lipid membranes are highly flexible and malleable interfaces, which behave as in-plane viscous fluids in physiological conditions. The interfacial fluidity and bending flexibility are crucial for many cellular functions involving membrane shape transformations, such as vesicular or tubular trafficking,[1] or shaping the cell organelles, and also for variety of dynamics observed in biomimetic systems.[2–6] The interfacial fluidity is also essential to the mobility of inclusions such as membrane proteins[7] or fluid domains,[8] the transport of lipids between cells through membrane tubes,[9] and lateral reorganizations, such as the formation of lipid rafts.[10] Other amphiphilic membranes such as polymersomes[11] also exhibit in-plane fluidity, with a hyper-viscous behavior.[12] Our goal here is to understand if and how shape deformations affect the lateral mobility of inclusions in fluid membranes.

The lateral motion of membrane probes subjected to stochastic or external forces has a long and rich history, dating back to the work of Saffman and Delbrück (SD).[7] This theory estimates the diffusion coefficient through the hydrodynamic mobility of an inclusion of size a in an inextensible membrane of interfacial viscosity μ_s embedded in bulk fluid of viscosity μ_b. For inclusions much smaller than the SD length scale $\ell_{SD} = \mu_s/\mu_b$, such as proteins in cell membranes, the mobility is inversely proportional to the interfacial viscosity μ_s, with a weak logarithmic dependence on ℓ_{SD}/a for infinite planar membranes. While the dependence on a is still controversial in some regimes,[13] it has been recently predicted theoretically[14] and verified experimentally with membrane tubes[15] that the mobility of probes is significantly modified by the membrane curvature. In short, highly curved membranes are geometrically confined and the correction in the mobility is $\ln(R/a)$ instead, where R is the radius of curvature of the curved membrane, in close correspondence with the SD estimate for membranes of finite size.

The SD theory and subsequent refinements, either considering planar[16–19] or curved membranes,[14,15] assume that the membrane geometry is fixed. Since the membrane rheology is assumed to be Newtonian, which is consistent with various experiments,[20,21] these theories predict a purely viscous lateral behavior. Here, by lifting this approximation and allowing the membrane to deform out-of-plane, we find that curved fluid membranes with bending elasticity behave laterally as an effective viscoelastic medium, and consequently exhibit much richer rheology, including frequency-dependent mobility, and non-zero storage modulus. At the root of this behavior, we show that the purely lateral motion of an inclusion produces

† Electronic Supplementary Information (ESI) available: [details of any supplementary information available should be included here]. See DOI: 10.1039/b000000x/

[a] *LaCàN, Universitat Politècnica de Catalunya-BarcelonaTech (UPC), Barcelona 08034, Spain.* [b] *SISSA–International School for Advanced Studies, Via Beirut 2-4, 34014 Trieste, Italy.* * *Corresponding author,Tel: +34-93-401-1805; E-mail: marino.arroyo@upc.edu*

shape disturbances in a curved membrane, which in turn couple the lateral behavior with the bending elasticity of the membrane. All these couplings are mediated by curvature and interfacial viscosity, and have escaped previous studies about membrane dynamics, which either assume fixed shapes or linearize the dynamical equations about planar states.[22] Even theoretical studies accounting for the effect of thermal undulations on the diffusion of inclusions, which we ignore here, predict purely viscous lateral behavior.[23,24] The curvature and frequency dependent probe mobility that we identify here can influence the way membrane-bound macromolecules or lipid domains diffuse in cell membranes of different geometries, and may help engineer interfacial processes in functionalized polymersomes.[25,26]

The mechanics of interfacial fluids necessarily involves the tools of differential geometry, and has been formulated in various ways since the early work of Scriven.[27,28] Here, we rely on and further expand a geometric formulation of the governing equations[29] in Section 2. At the end of this section, we provide a physical interpretation of the equations, which vividly show the tight coupling between shape dynamics, curvature elasticity, and interfacial hydrodynamics. To avoid loosing these couplings in the linear response, we then linearize the governing equations about a cylindrical geometry in Section 3. In Section 4, we make a connection with contemporary microrheology,[30,31] which could experimentally test our predictions, by adapting to the present setting the Generalized Stokes-Einstein relations linking viscoelastic rheology to the statistics of probe trajectories. We then illustrate the lateral response of a curve membrane by applying a tangential point force on a cylindrical membrane, in Section 5. We describe the anisotropy and viscoelasticity of the effective lateral behavior, analyze it from the viewpoint of microrheology, and examine its curvature dependence. We collect the conclusions in Section 6.

2 Mechanics of a viscous, curved, and evolving interface

We develop next a variational model for an inextensible Newtonian fluid interface with bending elasticity embedded in a bulk fluid in the limit of vanishing Reynolds number. We adopt here the common assumption of ignoring the membrane extensibility, and consequently disregard the bilayer architecture and the dissipative forces due to inter-monolayer friction,[22] which may nevertheless play an important role in some situations such as the extrusion of membrane tethers.[32] We have considered elsewhere a model including the bilayer architecture, and analyzed it by either linearizing it around curved geometries[33] or by performing fully nonlinear simulations.[34] However, for the purpose of the present work, such a complex model hides the key ideas without bringing additional insight.

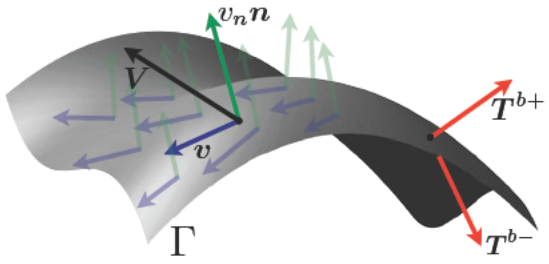

Fig. 1: Depiction of the dynamical fluid interface Γ. Assuming no-slip, the velocity of the surrounding fluid $\boldsymbol{V}$ at Γ is that of the interface, which is decomposed into a tangential component $\boldsymbol{v}$, describing the interfacial flow, and a normal component v_n along the unit normal to the surface $\boldsymbol{n}$, describing the shape changes. The bulk fluid exerts tractions on either sides of the interface, given by $\boldsymbol{T}^{b\pm} = \pm \boldsymbol{n} \cdot \boldsymbol{\sigma}^{b\pm}$, where $\boldsymbol{\sigma}^{b\pm}$ is the bulk stress tensor on the $+$ and $-$ sides of the membrane.

The fluid interface is represented by a surface Γ with unit normal $\boldsymbol{n}$. Its first and second fundamental forms are denoted by $\boldsymbol{g}$ and $\boldsymbol{k} = -\nabla_s \boldsymbol{n}$, where ∇_s is the surface nabla operator or covariant derivative. The components of the inverse of the metric tensor are denoted in a given coordinate system as g^{ij}, so that $g_{ik}g^{jk} = \delta_i^k$. The mean curvature (average of principal curvatures) is $H = (1/2)\boldsymbol{g} : \boldsymbol{k} = (1/2)g^{ij}k_{ij}$, while the Gaussian curvature (the product of the principal curvatures) can be computed as $K = \det(k_{ij}g^{jk})$.

The surface Γ is embedded in a bulk fluid. Assuming no-slip, the interface velocity $\boldsymbol{V}$ is that of the bulk fluid. We decompose $\boldsymbol{V}$ into a tangential component $\boldsymbol{v}$ describing the interfacial flow, and a normal component v_n describing shape changes of the interface, see Fig. 1. In this setting, the rate-of-deformation tensor takes the form[27–29]

$$\boldsymbol{d} = \frac{1}{2}\left(\nabla_s \boldsymbol{v} + \nabla_s \boldsymbol{v}^T\right) - v_n \boldsymbol{k}. \tag{1}$$

Consequently, the interface inextensibility condition reads

$$0 = \mathrm{trace}(\boldsymbol{d}) = \nabla_s \cdot \boldsymbol{v} - 2Hv_n, \tag{2}$$

which strongly couples shape changes and interfacial flows in the presence of curvature. Following a Boussinesq-Scriven model for an inextensible Newtonian fluid interface, the interfacial stress tensor reads $\boldsymbol{\sigma} = -\Sigma \boldsymbol{g} + 2\mu_s \boldsymbol{d}$, where μ_s is the interfacial viscosity and Σ is the scalar membrane tension keeping the inextensibility constraint.

The governing equations for the interfacial fluid dynamics can be elegantly deduced with variational methods, which also provide a framework for simpler numerical simulations and analytical calculations. Indeed, the analytical treatment of

the interfacial fluid mechanics for spherical or cylindrical geometries becomes particularly simple by using the dissipation functionals derived below and exploiting the vector calculus identities of vector spherical or cylindrical harmonics.[35] The Rayleigh dissipation potential for an inextensible interfacial viscous fluid can be expressed as[29,36]

$$W_{\mu_s} = \int_\Gamma \mu_s d : d \, dS. \tag{3}$$

As detailed in Appendix A this potential admits an alternative form, which highlights the geometry, the individual roles of v (interfacial flow) and v_n (shape changes), and involves the usual vector calculus surface operators (divergence, curl). For closed surfaces, we have

$$\begin{aligned} W_{\mu_s} = \int_\Gamma \mu_s \Big[& \frac{1}{2}|\nabla_s \times v|^2 + (\nabla_s \cdot v)^2 - K|v|^2 \\ & - 2v_n k : \nabla_s v + v_n^2 (4H^2 - 2K) \Big] \, dS, \end{aligned} \tag{4}$$

which grouping terms to annihilate $\nabla_s \cdot v - 2Hv_n$ due to local inextensibility becomes

$$\begin{aligned} W_{\mu_s} = \int_\Gamma \mu_s \Big[& \frac{1}{2}|\nabla_s \times v|^2 - K|v|^2 \\ & - 2v_n (k - 2Hg) : \nabla_s v - 2Kv_n^2 \Big] \, dS. \end{aligned} \tag{5}$$

The dynamics of the system can be obtained by minimizing the total Rayleigh dissipation potential, which also includes that of the bulk embedding fluid, plus the rate of change of the elastic energy of the interface with respect to the variables expressing the rate of change of the system,[37] possibly subject to constraints. Considering for simplicity an infinite embedding fluid without body forces, its dissipation potential can be written exclusively in terms of the velocity of the membrane, $W_{\mu_b}[v, v_n]$. On the other hand, the rate of change of the Helfrich bending energy $E = \int_\Gamma (\kappa/2) H^2 dS$, where κ is the bending modulus and we have ignored the spontaneous curvature for simplicity, depends only on the normal velocity $\dot{E}[v_n]$.[29] With all these ingredients, the tangential and normal Euler-Lagrange equations for the viscous interface with bending stiffness, together with the inextensibility constraint in Eq. (2), follow from annihilating the variations of

$$W_{\mu_b}[v, v_n] + W_{\mu_s}[v, v_n] + \dot{E}[v_n] - \int_\Gamma \Sigma (\nabla_s \cdot v - 2Hv_n) dS, \tag{6}$$

with respect to v, v_n, and Σ, and integrating by parts. Focusing on the role of the interfacial fluid (the bulk fluid and curvature elasticity contributions are classical), the tangential balance of linear momentum at the interface is

$$\begin{aligned} 0 = & -\mu_s [\nabla_s \times \nabla_s \times v - 2Kv + 2(k - 2Hg) \cdot \nabla_s v_n] \\ & - \nabla_s \Sigma + \left(t^{b+} + t^{b-} \right), \end{aligned} \tag{7}$$

where $t^{b\pm}$ is the tangential component of the traction exerted by the bulk fluid on the $+$ and $-$ sides of the membrane, see Fig. 1. It is interesting to note that the second and third terms of the interfacial viscous contribution (first line) vanish for planar membranes, and the third term vanishes for membranes of fixed geometry. For curved membranes of fixed shape,[14] the mobility of inclusions depends on curvature because of (1) the second interfacial viscous term, i.e. $-2\mu_s K v$, (2) the asymmetry of the bulk fluid tractions in a curved geometry, and (3) the topology of some curved geometries, e.g., cylinders or spheres, where the interfacial velocity field due to a localized force may not decay in the membrane perimeter. The viscous term depending on the gradient of the normal velocity and the curvature shows that non-uniform shape changes induce interfacial viscous tractions, and therefore influences the lateral mobility.

The balance of linear momentum normal to the membrane leads to the scalar equation

$$\begin{aligned} 0 = & -2\mu_s \left[k : \nabla_s v - (4H^2 - 2K) v_n \right] + 2H\Sigma \\ & - \left(t_n^{b+} - t_n^{b-} \right) + \kappa \left[\Delta_s H + 4H(H^2 - K) \right], \end{aligned} \tag{8}$$

where $t_n^{b\pm}$ are the normal components of the tractions exerted by the bulk fluid. The first term in this equation represents normal tractions due to the interfacial viscosity, the second term embodies Laplace's law, and the last term is the normal traction due to bending elasticity. Remarkably, the interfacial viscosity contribution completely vanishes at a planar configuration, which explains why this effect is generally neglected, e.g. when studying the dynamics of fluctuations.[22] The term $-2\mu_s k : \nabla_s v$ is a normal traction generated by a nonuniform interfacial flow in the presence of curvature, and clearly shows that the lateral motion of an inclusion in a curved fluid membrane generates a shape disturbance near the features of the associated interfacial flow. A crucial consequence of this observation is that, through curvature, the lateral interfacial hydrodynamics couple with the out-of-plane bending elasticity, which is at the root of the effective lateral viscoelastic behavior reported later. The second interfacial viscous term drags shape changes, which in turn influences the lateral mobility, and as we show elsewhere, can play a crucial role in the fluctuations of membranes of curvature close to or larger than ℓ_{SD}.[33] Figure 2 shows a simplified representation of the system under consideration, and how the lateral effective viscoelas-tic behavior emerges from a curvature-dependent coupling between lateral and out-of-plane motions. Note that, although in principle the bulk hydrodynamics could contribute to the coupling between lateral and normal dynamics in the presence of curvature, such contribution is negligible compared to that of the interfacial hydrodynamics. Indeed, for highly curved membranes and common inclusions, both the radius of curvature and the inclusion size are much smaller than ℓ_{SD}.

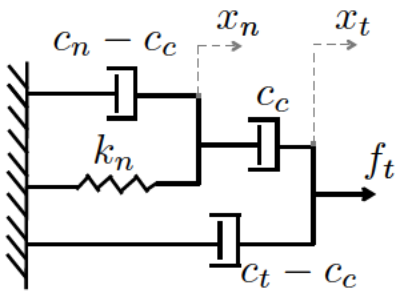

Fig. 2: Simplified rheological model illustrating the lateral mobility (x_t) of a membrane inclusion under the action of a lateral force f_t. In the absence of curvature, the coupling damper has no effect, $c_c = 0$, and therefore the lateral rheology is purely viscous, where c_t represents the net effect of the interfacial and bulk viscosities, whereas the out-of-plane motion x_n is viscoelastic due to bending elasticity, and bulk and interfacial viscosities. The coupling damping coefficient c_c becomes increasingly large with increasing curvature, which leads to a normal force exciting the viscoelastic out-of-plane response upon a purely lateral force on the inclusion. Thus, the lateral effective behavior is viscoelastic.

Thus, the physical origin of c_c is essentially the coupling term $-2\mu_s v_n k : \nabla_s v$ in the dissipation potential in Eq. (4).

3 Linearized governing equations for cylindrical membranes

We derive next the linearized equations around a cylindri-cal state using a variational method rather than the Euler-Lagrange equations, i.e. we minimize the Rayleigh dissipation potential plus the rate of change of elastic energy subject to inextensibility constraints. This method simplifies combining different physical mechanisms and eases the calculations. We have checked the resulting equations for the bulk flow and for the curvature energy with other works.[14,38] The interfacial flow equations have not been derived before and have been checked by computing in different ways the dissipation for a number of prescribed membrane velocity fields.

Disturbances around an equilibrium state

We linearize the model developed in Section 2 around an equilibrium cylindrical state, characterized by its radius r_0, its equilibrium surface tension Σ_0, and the equilibrium pressure difference across the membrane p_0. These three parameters should obey the relation $p_0 = -\kappa/(2r_0^3) + \Sigma_0/r_0$, encoding radial balance of forces.[6,38]

We parametrize the midsurface of a tubular membrane Γ at a given time t in cylindrical coordinates as

$$x(\theta,z;t) = r(\theta,z;t)e_r + ze_z, \tag{9}$$

where $\theta \in [0,2\pi]$, $z \in [0,L]$, and L is the length of the tube. We denote by e_r, e_θ, e_z the unit basis vectors of the cylindrical coordinates, and express the metric tensor, the normal vector, the second fundamental form, and the surface and volume elements as

$$\begin{aligned} &g_i = \partial_i x, \quad g_{ij} = g_i \cdot g_j, \quad i = \theta, z \\ &n = \frac{g_\theta \times g_z}{|g_\theta \times g_z|}, \quad k_{ij} = \partial_{ij} x \cdot n \\ &dS = |g_\theta \times g_z|\, d\theta dz, \quad dV = \frac{r^2}{2}\, d\theta dz dr. \end{aligned} \tag{10}$$

We call u the shape disturbances from the equilibrium cylindrical state, $r(\theta,z;t) = r_0 + u(\theta,z;t)$, and represent it with a Fourier expansion,[38]

$$u(\theta,z;t) = \sum_{n,m} u_{nm}(t) Y_{nm}(\theta,z), \tag{11}$$

where $Y_{nm}(\theta,z) = e^{i(m\theta + k_n z)}$, $k_n = 2n\pi/L$, and m, n are integers running from $-\infty$ to $+\infty$. From this point on, we drop the explicit dependence on time of the coefficients in the various expansions. Similarly, we expand the surface velocity as

$$V = \sum_{n,m} \left(v^r_{nm} e_r + v^\theta_{nm} e_\theta + v^z_{nm} e_z \right) Y_{nm}. \tag{12}$$

Note that $\dot{u}_{nm} = v^r_{nm}$. Alternatively, it is convenient to expand this field differently to compute the interfacial dissipation. In analogy with vector spherical harmonics,[35] we describe the surface velocity field with vector cylindrical harmonics

$$V = \sum_{n,m} \left(v^r_{nm} \mathbf{Y}_{nm} + v^{(1)}_{nm} \mathbf{\Psi}_{nm} + v^{(2)}_{nm} \mathbf{\Phi}_{nm} \right), \tag{13}$$

where $\mathbf{Y}_{nm}(\theta,z) = Y_{nm} e_r$, $\mathbf{\Psi}_{nm}(\theta,z) = r_0 \nabla_s Y_{nm}$, and $\mathbf{\Phi}_{nm} = e_r \times \mathbf{\Psi}_{nm}$. Some mathematical properties of vector cylindrical harmonics are given in Appendix B. We define the following arrays containing the components in these two representations

$$\mathbf{V}_{nm} = \begin{Bmatrix} v^r_{nm} \\ v^\theta_{nm} \\ v^z_{nm} \end{Bmatrix}, \quad \mathbf{W}_{nm} = \begin{Bmatrix} v^r_{nm} \\ v^{(1)}_{nm} \\ v^{(2)}_{nm} \end{Bmatrix},$$

which are related by

$$\mathbf{W}_{nm} = \underbrace{\begin{bmatrix} 1 & 0 & 0 \\ 0 & im/\lambda_{nm} & ik_n r_0/\lambda_{nm} \\ 0 & -ik_n r_0/\lambda_{nm} & im/\lambda_{nm} \end{bmatrix}}_{\mathbf{B}_{nm}} \mathbf{V}_{nm}, \tag{14}$$

where $\lambda_{nm} = r_0^2 k_n^2 + m^2$.

Membrane free energy

The free energy of an inextensible membrane, including the bending energy and the work of pressure and surface tension can be written as

$$\Pi = \frac{\kappa}{2}\int_\Gamma (2H)^2 dS + \Sigma_0 \int_\Gamma dS - p_0 \int_V dV, \tag{15}$$

where V is the volume enclosed by the membrane. By introducing the expansion in Eq. (11), retaining up to second order terms, and noting that linear terms vanish since we linearize about an equilibrium state, we obtain the harmonic expansion of the free energy (see Appendix C)

$$\Pi = \Pi_0 + \frac{1}{2}\sum_{n,m} u^*_{nm} E_{nm} u_{nm}, \tag{16}$$

where $()^*$ denotes complex conjugation and conjugate transposition for matrices, $E_{nm} = 2\pi L\left(\kappa q_{nm}/r_0^3 - p + \Sigma\lambda_{nm}/r_0\right)$, and $q_{nm} = -\lambda_{nm}/2 + \lambda_{nm}^2 - m^2 + 1$. It follows immediately that

$$\dot{\Pi} = \frac{1}{2}\sum_{n,m}\left(u^*_{nm}E_{nm}v^r_{nm} + u_{nm}E_{nm}v^{r*}_{nm}\right), \tag{17}$$

Note that the stability of the equilibrium state holds if $E_{nm} > 0$ for all n and m. This is always the case if $p_0 = 0$, as considered in all the examples of the paper.

Inextensibility

The dynamical equations of inextensible fluid membranes should satisfy the local mass conservation constraint in Eq. (2). The surface tension deviation from Σ_0

$$\hat{\Sigma}(\theta,z) = \Sigma(\theta,z) - \Sigma_0 = \sum_{n,m}\Sigma_{nm}Y_{nm}(\theta,z), \tag{18}$$

acts a Lagrange multiplier for this constraint, which is enforced variationally with the expression

$$C^{\text{inext}} = \int_\Gamma \hat{\Sigma}\left(\nabla_s\cdot\boldsymbol{v} - 2v_n H\right) dS. \tag{19}$$

With the identities in Appendix B, the linearized form of the equation above is

$$\begin{aligned} C^{\text{inext}} &= 2\pi r_0 L\sum_{nm}\Sigma_{nm}\left(-\lambda_{nm}v^{(1)}_{nm}/r_0 - v^r_{nm}/r_0\right) \\ &= 2\pi r_0 L\sum_{nm}\Sigma_{nm}\left(imv^\theta_{nm}/r_0 + ik_n v^z_{nm} - v^r_{nm}/r_0\right), \end{aligned} \tag{20}$$

where we have used Eq. (14) in the last step.

Interfacial dissipation

Replacing the vector cylindrical harmonic expansion of the interfacial velocity in Eq. (13) into Eq. (4), taking advantage of the expressions in Appendix B, and mapping back to the usual Fourier expansion of the velocity with Eq. (14), we express the membrane interfacial dissipation potential at the cylindrical equilibrium state as

$$W_{\mu_s} = \frac{1}{2}\sum_{n,m}\mathbf{V}^*_{nm}\mathbf{D}^{\text{mem}}_{nm}\mathbf{V}_{nm}, \tag{21}$$

where

$$\frac{\mathbf{D}^{\text{mem}}_{nm}}{2\mu_s\pi r_0 L} = \mathbf{B}^*_{nm}\begin{bmatrix} 2/r_0^2 & 2m^2/r_0^2 & -2k_n m/r_0 \\ 2m^2/r_0^2 & 2\lambda^2_{nm}/r_0^2 & 0 \\ -2k_n m/r_0 & 0 & \lambda^2_{nm}/r_0^2 \end{bmatrix}\mathbf{B}_{nm}.$$

Bulk dissipation

A general solution to the 3D Stokes equations in cylindrical coordinates is given by,[39]

$$\begin{aligned} \boldsymbol{V}^{b\pm}(r,\theta,z) =& \nabla f^\pm(r,\theta,z) + \nabla\times\left[g^\pm(r,\theta,z)\boldsymbol{e}_z\right] \\ &+ r\partial_r\left[\nabla h^\pm(r,\theta,z)\right] + \partial_z h^\pm(r,\theta,z)\boldsymbol{e}_z, \\ p^\pm(r,\theta,z) =& -2\mu_b\partial_z^2 h^\pm(r,\theta,z), \end{aligned} \tag{22}$$

where ∇ is the bulk nabla operator, and $f^\pm(r,\theta,z)$, $g^\pm(r,\theta,z)$, $h^\pm(r,\theta,z)$ are cylindrical harmonic functions given by

$$\begin{Bmatrix} f^\pm(r,\theta,z) \\ g^\pm(r,\theta,z) \\ h^\pm(r,\theta,z) \end{Bmatrix} = \sum_{n,m}\begin{Bmatrix} F^\pm_{nm} \\ G^\pm_{nm} \\ H^\pm_{nm} \end{Bmatrix} P^\pm_m(k_n,r)Y_{nm}(\theta,z). \tag{23}$$

Here, $P^\pm_m(k_n,r)$ denote modified Bessel functions of the second and first kind, i.e. $P^+_m = K_m(|k_n|r)$ and $P^-_m = I_m(|k_n|r)$. Since $\lim_{x\to 0}K_m(x) = \lim_{x\to\infty}I_m(x) = +\infty$, the modified Bessel functions of the first and second kind are appropriate solutions for the exterior and interior bulk fluid, respectively. We can calculate the coefficients of the harmonic functions (F, G, and H) by imposing the non-slip boundary conditions on the surface. Expressing the bulk fluid velocity surrounding the cylindrical surface as $\boldsymbol{V}^{b\pm} = V^{b\pm}_r\boldsymbol{e}_r + V^{b\pm}_\theta\boldsymbol{e}_\theta + V^{b\pm}_z\boldsymbol{e}_z$, and recalling Eq. (22), we have

$$\begin{aligned} V^{b\pm}_r =& \partial_r f^\pm + \frac{1}{r}\partial_\theta g^\pm + r\partial^2_{rr}h^\pm, \\ V^{b\pm}_\theta =& \frac{1}{r}\partial_\theta f^\pm - \partial_r g^\pm - \frac{1}{r}\partial_\theta h^\pm + \partial^2_{\theta r}h^\pm, \\ V^{b\pm}_z =& \partial_z f^\pm + r\partial^2_{zr}h^\pm + \partial_z h^\pm. \end{aligned} \tag{24}$$

Combining Eqs. (23), (24) and (12), the bulk and surface velocities can be related through the coefficients of the harmonic

functions as

$$\left\{ \begin{array}{c} F^{\pm}_{nm} \\ G^{\pm}_{nm} \\ H^{\pm}_{nm} \end{array} \right\} = \left(\mathbf{Q}^{\pm}_{nm}\right)^{-1} \mathbf{V}_{nm}, \tag{25}$$

where the components of $\mathbf{Q}^{\pm}_{nm}$ are given in Appendix D.

The traction vector acting on the surface of a tube in cylindrical coordinates for an incompressible Newtonian fluid is,[39]

$$\boldsymbol{T}^{b\pm} = \pm \boldsymbol{e}_r \cdot \boldsymbol{\sigma}^{b\pm} = \pm \left[\begin{array}{c} -p^{\pm} + 2\mu_b \partial_r V^{b\pm}_r \\ \mu_b r \partial_r \left(V^{b\pm}_\theta / r\right) + \mu_b \partial_\theta (V^{b\pm}_r)/r \\ \mu_b \left(\partial_z V^{b\pm}_r + \partial_r V^{b\pm}_z\right) \end{array} \right].$$

Replacing Eqs. (24,25) into the above relation, we find

$$\boldsymbol{T}^{b\pm} = \pm \mu_b \sum_{nm} Y_{nm} \mathbf{S}^{\pm}_{nm} \left(\mathbf{Q}^{\pm}_{nm}\right)^{-1} \mathbf{V}_{nm}, \tag{26}$$

where the nonzero components of $\mathbf{S}^{\pm}_{nm}$ are given in Appendix D. From Eq. (26), the dissipation potential for the bulk fluid in the absence of body forces can be written as

$$W_{\mu_b} = -\frac{1}{2} \int_\Gamma \boldsymbol{V} \cdot \boldsymbol{T}^{b\pm} \, dS = \frac{1}{2} \sum_{nm} \mathbf{V}^*_{nm} \mathbf{D}^{\text{bulk}\pm}_{nm} \mathbf{V}_{nm}, \tag{27}$$

where $\mathbf{D}^{\text{bulk}}_{nm} = 2\pi r_0 L \mu_b \left[-\mathbf{S}^{+}_{nm} \left(\mathbf{Q}^{+}_{nm}\right)^{-1} + \mathbf{S}^{-}_{nm} \left(\mathbf{Q}^{-}_{nm}\right)^{-1} \right]$. The final expressions for the components of the dissipation matrix $\mathbf{D}^{\text{bulk}}_{nm}$, which is Hermitian, are given in Appendix D.

Linearized governing equations

As in Section 2, we obtain the dynamics of the system by minimizing the rate of change of free energy, plus the total dissipation potential, plus the power of the external forces with respect to the variables expressing the rate of change of the system and subject to constraints (here inextensibility). For this purpose, we form the Lagrangian $\mathscr{L}(\mathbf{V}_{nm}, \Sigma_{nm}) = \dot{\Pi}[\mathbf{V}_{nm}] + W^{\text{tot}}[\mathbf{V}_{nm}] + \dot{\Pi}^{\text{ext}}[\mathbf{V}_{nm}] + C^{\text{inext}}[\mathbf{V}_{nm}, \Sigma_{nm}]$ collecting Eqs. (17,21,27,20). Expressing the external force with Fourier expansion $\boldsymbol{f}^{\text{ext}}(\theta, z, t) = \sum_{nm} \boldsymbol{f}^{\text{ext}}_{nm}(t) Y_{nm}(\theta, z)$, we can express the external power as $\dot{\Pi}^{\text{ext}} = \sum_{nm} \mathbf{V}^*_{nm} \mathbf{f}^{\text{ext}}_{nm}$, where $\mathbf{f}^{\text{ext}}_{nm} = 2\pi r_0 L \boldsymbol{f}^{\text{ext}}_{nm}$. Making the Lagrangian stationary, we obtain a set of algebraic-differential equations

$$\left[\begin{array}{cc} \mathbf{D}^{\text{tot}}_{nm} & \mathbf{L}_{nm} \\ \mathbf{L}^T_{nm} & \mathbf{0} \end{array} \right] \left\{ \begin{array}{c} \mathbf{V}_{nm} \\ \Sigma_{nm} \end{array} \right\} = \left\{ \begin{array}{c} \mathbf{f}_{nm} + \mathbf{f}^{\text{ext}}_{nm} \\ 0 \end{array} \right\}, \tag{28}$$

where $\mathbf{D}^{\text{tot}}_{nm} = \mathbf{D}^{\text{bulk}}_{nm} + \mathbf{D}^{\text{mem}}_{nm}$, $\mathbf{f}^T_{nm} = \left[\begin{array}{ccc} -E_{nm} u_{nm} & 0 & 0 \end{array} \right]$, and $\mathbf{L}^T_{nm} = 2\pi r_0 L \left[\begin{array}{ccc} -1/r_0 & im/r_0 & ik_n \end{array} \right]$. Inverting the matrix in the left-hand-side and recalling that $v^r_{nm} = \dot{u}_{nm}$, the governing equations in Eq. (28) can be expressed as

$$\left\{ \begin{array}{c} \dot{u}_{nm} \\ v^{\theta}_{nm} \\ v^{z}_{nm} \\ \Sigma_{nm} \end{array} \right\} = \left\{ \begin{array}{c} k^r_{nm} \\ k^{\theta}_{nm} \\ k^{z}_{nm} \\ k^{\Sigma}_{nm} \end{array} \right\} u_{nm} + \left\{ \begin{array}{c} g^r_{nm} \\ g^{\theta}_{nm} \\ g^{z}_{nm} \\ 0 \end{array} \right\}, \tag{29}$$

where the coefficients denoted by k and g follow from simple algebraic calculations. The first row can be easily be integrated to an exponential function of time, and the remaining algebraic equations provide the tangential velocities and surface tension disturbances.

4 Probe mobility and membrane rheology

The SD theory assumes a purely viscous drag to motion, and relates through the Stokes-Einstein relation the diffusion coefficient to the viscosity of the embedding medium. Modern microrheology generalizes the Stokes-Einstein relations to linear viscoelastic (LVE) media,[30] and provides a link between the statistical properties of the motion of probes beyond simple diffusion, e.g., the mean squared displacement ($MSD(t) = \langle \Delta r^2(t) \rangle$), and the rheology of the medium. The hydrodynamical mobility, which can be probed under either an external force (active microrheology), or stochastic thermal forces (passive microrheology), becomes frequency-dependent for a general LVE medium.[31] The theory summarized below provides a precise mapping between the measurements of active and passive microrheology. We exploit this correspondence in Section 5, where we calculate the lateral response to an applied force, evaluate the effective viscoelastic behavior, and then reconstruct a typical measurement of passive microrheology, the MSD.

The hydrodynamic mobility M is generalized for LVE materials as[40]

$$v^P(t) = \int_{-\infty}^{t} M(t - t') f^P(t') \, dt',$$

where f^P is the force applied on the probe, here the membrane inclusion, and $v^P(t)$ is the velocity of the probe. For a purely viscous medium, the response to a force is instantaneous. By taking the Laplace transform of the previous equation, we can compute the frequency-dependent mobility of the probe from the applied force and the response as

$$\tilde{M}(s) = \tilde{v}^P(s) / \tilde{f}^P(s), \tag{30}$$

where s is the Laplace frequency, and the Laplace-transformed functions are denoted by a tilde. From fluctuation-dissipation, the translational mobility of a probe in N dimensions and the MSD are related by[31]

$$\widetilde{MSD}(s) = \frac{2Nk_BT}{s^2} \tilde{M}(s). \tag{31}$$

Given the frequency-dependent mobility, we introduce an effective lateral viscoelastic modulus. The theory behind interfacial microrheology is not fully established. To account for the fact that we deal with a two-dimensional medium, we

modify the usual bulk relations relating mobility to viscoelastic modulus[31] following the SD theory. Since for a bulk viscous medium $M \propto (\mu_b a)^{-1}$, while for a membrane inclusion $M \propto (\mu_s)^{-1}$, a dimensionally correct interfacial viscoelastic modulus follows from $\tilde{G}(s) = s/\tilde{M}(s)$. Replacing s by $i\omega$, we obtain the complex viscoelastic modulus of an equivalent two-dimensional medium as $G(\omega) = G'(\omega) + iG''(\omega)$. The real part G' is the storage modulus and G'' the loss modulus char-acterizing the elastic and viscous components of the medium under an oscillatory force.

5 Results

To show that a nonuniform interfacial flow generates shape deformations on a curved membrane, and examine the consequences of this effect on the lateral mobility, we consider a cylindrical membrane and subject it to a tangential point force in either the longitudinal or the azimuthal direction, in a set-up previously employed in membranes of fixed shape.[14] The point force is implemented by imposing a Dirac delta distribution in space at $z = 0$, and $\theta = 0$, and a Heaviside step function in time, i.e. $f^{\text{ext}}(\theta, z, t) = \delta(\theta)\delta(z)H(t)(f_\theta e_\theta + f_z e_z)$, where f_θ, and f_z are constants. The Fourier expression of the external force then can be written as $f^{\text{ext}}_{nm} = 2H(t)(f_\theta e_\theta + f_z e_z)/\pi L$. Following Henle and Levine,[14] we limit the number of Fourier modes in accordance to a cut off length scale $\ell_c \approx a$ representing the size of the inclusion as $n_{\max} = L/(2\pi\ell_c)$, $m_{\max} = r_0/\ell_c$. Thus, this problem has three length-scales. We place ourselves in the regime where ℓ_c is much smaller than ℓ_{SD} and smaller than r_0. In the calculations below, we choose $\ell_c = 10^{-3}\ell_{SD}$, and L long enough so that the disturbances created by the point force have decayed at the tube ends. We check that the rheological properties are insensitive to further increasing L.

We non-dimensionalize energy by κ, and length by $\ell_{SD} = \mu_s/\mu_b$. The non-dimensional radius is then $\bar{r} = r_0/\ell_{SD}$. For fixed geometry, the purely viscous system reacts instantaneously to the applied force because of the absence of inertia or elasticity.[14] Here, elasticity introduces a time-dependent response with a characteristic relaxation time. To have relaxation times close to one, we consider the following radius-dependent time-scale $\tau = 8r_0^2(\mu_s + 2\mu_b r_0)/\kappa = 8\bar{r}^2(1+2\bar{r})\tau_0$, where $\tau_0 = \ell_{SD}^3\mu_b/\kappa$.[33] For highly curved tubes, $\bar{r} \ll 1$, we have $\tau \approx 8r_0^2\mu_s/\kappa$, which is independent of the bulk viscosity. For phospholipids in water, ℓ_{SD} is on the order of a few μm, while for polymersomes ℓ_{SD} is in the order of mm. For a tube of radius $r_0 = 1$ μm, the characteristic time τ is 0.5 s for a phospholipid fluid membrane and around six minutes for a fluid polymersome.

Hydrodynamics and shape deformation

Figure 3 presents the transient response of the system to a point-load, in either the longitudinal or the azimuthal direction. We consider two tubes of different radii. The transient response is illustrated by plotting three selected snapshots of the shape, the interfacial velocity field, and the surface tension at $t = 0$, when the shape has not changed, at $t = +\infty$, when the system has reached steady state, and at an intermediate time. In all cases, there is a clear correlation between the interfacial hydrodynamics and the shape deformations. The membrane exhibits a negative out-of-plane displacement relative to the outer normal ahead of the point load, where the surface tension disturbance is negative, and a positive out-of-plane displacement behind the point load. As noted previously,[14] the velocity field on the surface is more localized relative to r_0 for larger tubes, since the decay length-scale is $\sqrt{r_0\ell_{SD}}$. The shape deformation as a result of f_z is more markedly non-axisymmetric for larger tubes, since modes that deform the cross-section become softer as r_0 increases. Our calculations show that for phospholipid membranes ($\kappa = 10^{-19}$ J), the typical lateral force exerted by a molecular motor ($f_z \approx 1$ pN)[41] can induce shape deformations whose maximum amplitude is about 0.05 r_0 for a tube of $r_0 = 50$ nm.

In Figure 4, we report more details about the dynamics of the interfacial velocity field for a tube of radius $r_0 = 0.02\ \ell_{SD}$. Figure 4(a) shows the transient velocity of the inclusion, a signature of an effective viscoelastic lateral response. The maximum velocity of the particle occurs at $t = 0$, when the force is applied and the membrane is not deformed, and then attains the steady state in a time-scale commensurate to τ, which is a significantly shorter (more than one order of magnitude) for the azimuthal motion. Thus, the inclusion encounters initially less resistance to motion as compared to later at steady state. Interestingly, the simple rheological model in Fig. 2 exhibits a similar behavior. It can be observed that for this small radius, v_z under a longitudinal force does not fully decay in the azimuthal direction, and exhibits back-flow on the side opposite to the point where the force is applied at $t = +\infty$ (a-3). This effect explains part of the radius dependence of the purely viscous steady-state rheology, more specifically the $\ln r_0$ dependence of mobility. Similarly, v_θ resulting from f_θ does not decay in the tube perimeter. For large tubes, which exhibit radius-independent behavior, these effects are absent. We note that at steady state, the membrane undergoes no shape changes, $v_n = 0$ in (a-4) and (b-4), and thus the response of the viscoelastic linearized system is equivalent to that of a tube of fixed geometry.[14]

Frequency dependent rheology

Having seen that the lateral behavior of a curved deformable fluid membrane is viscoelastic, we now quantify this re-

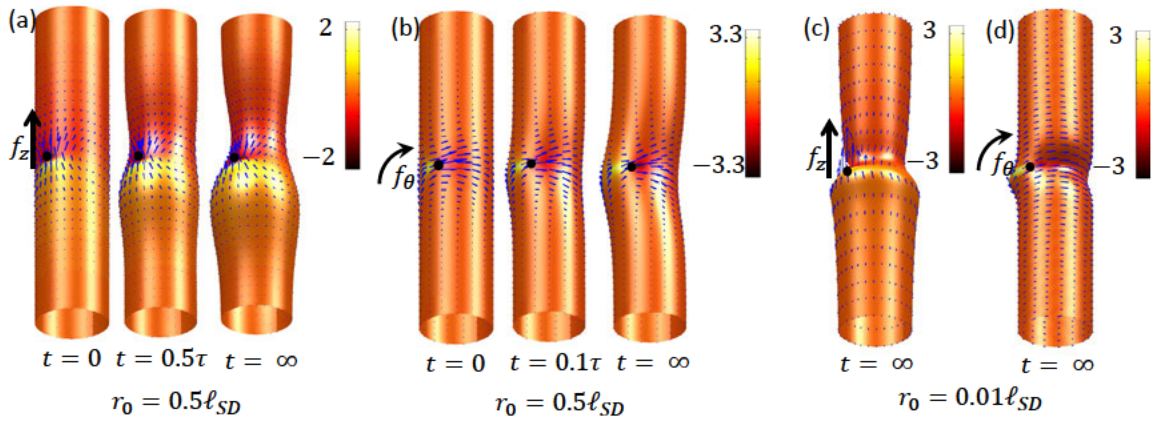

Fig. 3: Transient response of a tubular fluid membrane immersed in a viscous bulk fluid subjected to a tangential point force in the longitudinal (a,c) and azimuthal (b,d) direction. Here and in all other examples, the pressure difference p_0 is zero. We represent the interfacial flow (blue arrows), the shape disturbances, and the membrane tension deviations from Σ_0 (color map, in units of $10^3 f/\ell_{SD}$). The out-of-plane disturbances have been amplified by a factor of about 20 $\kappa/(f\ell_{SD})$ (a,b), and 200 $\kappa/(f\ell_{SD})$ (c,d), and the tubes have been rescaled in the longitudinal direction by a factor of 1 (a,b) and 1/6 (c,d).

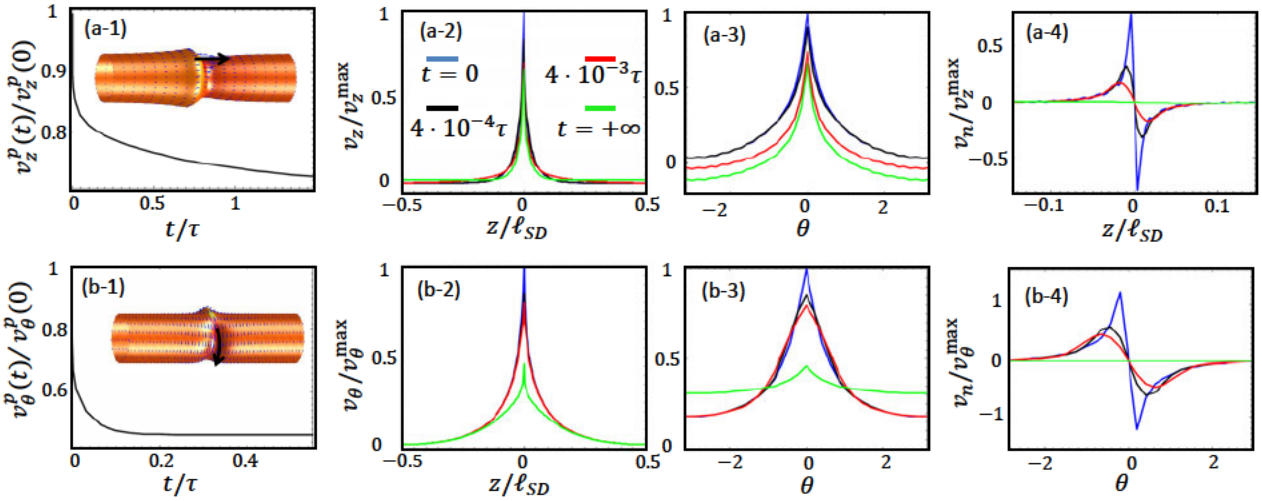

Fig. 4: Dynamical response of a thin tube of radius $r_0 = 0.02\ \ell_{SD}$ upon (a) longitudinal and (b) azimuthal point forces. (1) In-plane velocity of the inclusion, or probe velocity v_i^P, as a function of time. (2) Longitudinal profile of the in-plane velocity passing through the inclusion, (3) azimuthal profile of the in-plane velocity passing through the particle, and (4) longitudinal (a)/azimuthal (b) profile of the normal velocity passing through the inclusion, at different time instances.

sponse invoking the generalized Stokes-Einstein relations[31] summarized in Section 4. Since the mobility of the inclusion is strongly anisotropic, we treat separately the longitudinal and the azimuthal response, and consequently take $N = 1$ in Eq. (31). Recalling Eq. (30) and substituting $\tilde{f}_z^P(s) = f_z/s$, and $\tilde{f}_\theta^P(s) = f_\theta/s$ since the applied force is a Heaviside step function in time, we have

$$\tilde{M}_i(s) = s/\tilde{G}_i(s) = \frac{s^2\widetilde{MSD}_i(s)}{2k_BT} = \frac{s\tilde{v}_i^P(s)}{f_i}, \quad i = z,\theta. \tag{32}$$

Therefore, we can calculate the mean squared displacement in the time-domain as

$$MSD_i(t) = (2k_BT/f_i)\int_0^t v_i^P(t)dt, \quad i = z,\theta. \tag{33}$$

The frequency-dependent and anisotropic lateral rheology of a curved and deformable cylindrical membrane of radius $r_0 = 0.02\ \ell_{SD}$ is shown in Figure 5. The system behaves like an effective linear viscoelastic (LVE) medium, which we compare with the purely viscous (PV) response of a membrane of

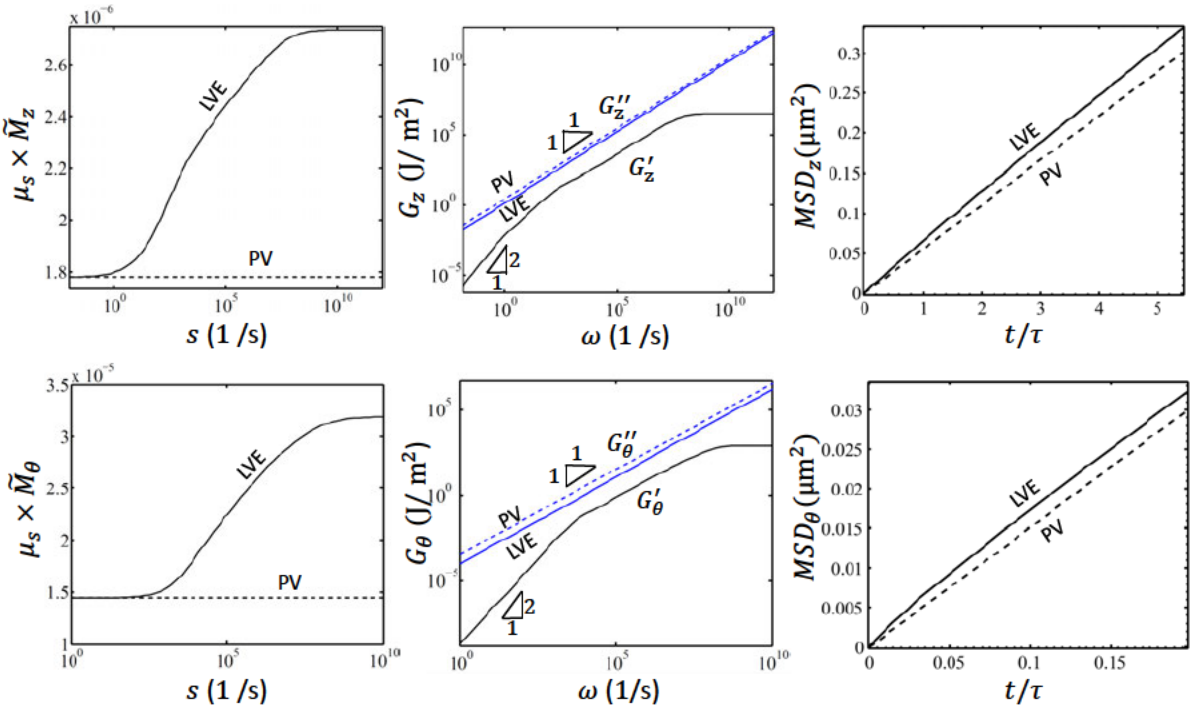

Fig. 5: Frequency-dependent lateral rheological properties (left: mobility in the Laplace domain, middle: storage and loss moduli in the Fourier domain, right: MSD as a function of time) of a tubular membrane in the longitudinal (top row) and azimuthal (bottom row) directions. In this figure, we select specific material parameters representative of a phospholipid membrane in the fluid phase in water: $\kappa = 10^{-19}$ J, $\ell_{SD} = 5$ μm, and $\tau = 4.2$ ms. The tube radius is $r_0 = 0.02\,\ell_{SD} = 100$ nm. The linear viscoelastic (LVE) behavior of the deformable membrane is represented by solid lines, while the purely viscous (PV) response of a tube of fixed geometry is represented by dashed lines for comparison.

fixed geometry. Examining first the mobility of the viscoelastic deformable system as a function of Laplace frequency (left panels), we observe that the mobility transitions from the PV behavior of the rigid system at low frequencies (steady state) to a significantly higher plateau at high frequencies. The total increase of mobility is about two-fold for this example. This result may have experimental implications, as it suggests that the mobility measured in the low-frequency limit, e.g., by active microrheology under constant force, should differ significantly from that operative in high frequencies, due for instance to stochastic thermal forces, and probed with different experimental techniques. The longitudinal and azimuthal behavior is qualitatively very similar. As for the viscoelastic complex modulus (middle column), the system exhibits a loss modulus that approximately follows $G'' \propto \omega$, and is noticeably smaller than that of the PV system, particularly for low frequencies (about two times smaller along z and three times smaller along θ). More interestingly, the storage modulus G' of the LVE model displays more structure with three different regimes separated by two characteristic frequencies. It is constant at high frequencies, follows $G' \propto \omega^2$ at low frequencies, and exhibits a more complex behavior that approximately follows $G' \propto \omega$ for $\omega \in (\omega^*, \omega^{**})$. These two characteristic frequencies can also be observed in the mobility plots in the left panels. We observe that the behavior is dominantly viscous at all frequencies, as quantified by the phase-lag angle δ, defined by $\tan\delta = G''/G'$. The ratio G''/G' attains its maximum, in the order of 10 for this tube, close to ω^*. Many of these features are also present in the simple rheological model in Fig. 2, which nevertheless has only one time-scale and therefore the intermediate regime $G' \propto \omega$ is absent. Indeed, for this model

$$G' = \frac{c_c^2 k_n \omega^2}{c_n^2\omega^2 + k_n^2}, \quad G'' = c_t\omega - \frac{c_c^2 c_n \omega^3}{c_n^2\omega^2 + k_n^2}, \tag{34}$$

where the PV behavior is recovered by setting $c_c = 0$, $k_n = +\infty$, or $\omega = 0$. We finally report the predicted MSD, which could be measured with sufficient resolution to capture the systematic deviation from the simple diffusive behavior as a signature of viscoelasticity. In both the longitudinal and the azimuthal directions, $MSD(t)$ is concave and progressively reaches the linear dependence on time.

The two characteristic frequencies ω^* and ω^{**} arise from two independent length scales, the tube radius r_0 and the inclusion size a. The first characteristic frequency is proportional to

the inverse of the relaxation time-scale defined earlier, $\omega^* \propto 1/\tau$. For $r_0 \ll \ell_{SD}$, we check that $\omega_z^* \approx 1/\tau \approx \kappa/(8\mu_s r_0^2)$, while in the azimuthal direction ω_θ^* is about one order of magnitude faster, as already noted in Fig. 4-1. The higher characteristic frequency stems scales as $\omega^{**} \propto \kappa/(\mu_s a^2)$. Figure 6 examines the dependence of the ratio G_z''/G_z' on tube radius and inclusion size. It can be observed that indeed ω^* and ω^{**} decrease as r_0 and a increase, respectively. Therefore, the width of the $G' \propto \omega$ regime, where viscoelasticity is more pronounced, scales with r_0/a. Conversely, it can be appreciated that the peak viscoelastic response, measured as

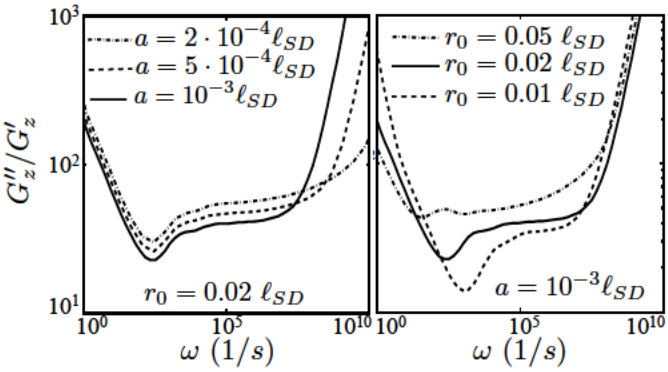

Fig. 6: Dependence of the ratio $G_z''(\omega)/G_z'(\omega)$ on the inclusion size a (left) and on the tube radius r_0 (right).

We now examine the dependence of rheology on tube radius relative to ℓ_{SD} at fixed inclusion size. As a measure representative of the rheology in the high and low-frequency limits, we consider the two horizontal asymptotes of $\tilde{M}_i(s)$, see Fig. 5, left column. The lower asymptote, for low Laplace frequencies, coincides with the purely viscous and frequency-independent mobility in a cylindrical membrane of fixed geometry, while the larger asymptotic mobility at high frequencies reflects the viscoelastic nature of the deformable membrane. For large radii, as shown in Figure 7, all mobilities collapse to the SD estimate for planar infinite membranes (dashed red line). The low frequency/purely viscous behavior (blue squares) reflects the $\ln(r_0/a)$ dependence of the SD estimate for membranes of finite size. As shown in the figure, the viscoelastic response at high frequencies (black circles) of the deformable system progressively deviates from the low frequency response as the radius decreases. The high-frequency mobility of the viscoelastic deformable system can differ from that of the purely viscous rigid system by a factor of 2 for $r_0 = 10^{-2}\ell_{SD}$.

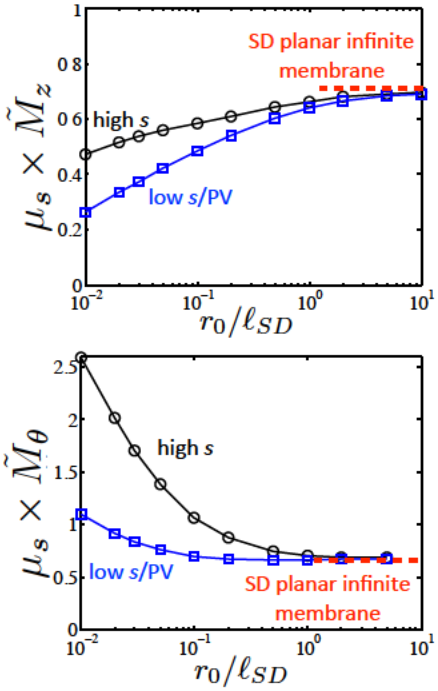

Fig. 7: Dependence of the mobility in the high (black circles) and low (blue squares) frequency limits on the radius of the tube, in the longitudinal (top) and azimuthal (bottom) directions. The low-frequency limit coincides with the purely viscous (PV) behavior of a tubular membrane with fixed shape. The dashed red line shows the SD estimate for the mobility in an infinite planar membrane.

6 Conclusion

We have shown that curved fluid membranes behave laterally as an effective viscoelastic medium, even if the membrane fluidity is purely viscous. Consequently, the lateral mobility of a membrane inclusion is frequency-dependent, and the effective storage modulus is non-zero. At the root of this result is the observation that the lateral motion of a probe generates a non-uniform interfacial flow, which in the presence of curvature creates a shape deformation mobilizing the out-of-plane viscoelastic response. To capture this effect, two theoretical ingredients developed here are essential: (1) a general formulation of the interfacial hydrodynamics at finite curvature, and (2) the linearization of the governing equations around a curved state.

This result may provide new insights in the diffusion of membrane proteins or membrane domains in the highly curved and heterogeneous environment of cell organelles, or in cell-cell communication through membrane nanotubes.[42] The physical mechanisms identified here could also help reconcile mobility measurements in lipid bilayers obtained with techniques probing different time-scales.[43] From a techno-

logical perspective, our results may be particularly relevant to understand interfacial processes of functionalized polymersomes,[25,26] which hold great promise as drug-delivery carriers, biosensors, or nanoreactors.[44,45]

The effect identified here can in principle be observed in lipid bilayer tubes, although the experimental resolution of recent related experiments[15] may be insufficient to discern it. As shown by our results, the viscoelastic behavior is stronger for tubes of small radius relative to the SD length-scale, and for large inclusions. Polymersomes, with ℓ_{SD} in the millimeter range, appear as an ideal model system to experimentally interrogate the lateral viscoelasticity of fluid membranes of different curvatures with mircorheological techniques. In these systems, it may even be possible to observe the shape disturbances under an applied lateral force.

A number of variations on the model analyzed here can be envisaged, including spherical geometries, or bulk fluids of different viscosity on either side of the membrane. Our theory can be combined with refinements of the SD theory, such as those accounting for the shape of the inclusion, e.g. in terms of hydrophobic mismatch[46] or intrinsic curvature,[47] which have been shown to modify the purely viscous response without in-troducing a qualitatively different rheological behavior. The case of membrane curving inclusions is particularly intriguing since, even in a nominally planar bilayer, they locally pro-duce curvature and therefore effects similar to those reported in here are likely to play a role. The theory developed here can also be extended to account for the bilayer architecture, i.e. the monolayer extensibility and the inter-monolayer fric-tion. From our preliminary calculations, such effects may only become significant for inclusions spanning only one mono-layer, but this issue deserves further study. To ascertain the dependence of the viscoelastic behavior on curvature, probe size, or material parameters, it would be particularly useful to particularize the theory in different asymptotic regimes and obtain explicit expressions. Finally, here and in most studies, the mobility of probes under the action of stochastic thermal forces is analyzed assuming that the background medium is not fluctuating, invoking scale separation between the probe and the solvent molecules. However, membrane fluctuations can be significant and span a wide range of time and length scales. Several studies have shown that the fluctuations can modify noticeably the diffusion coefficient in a purely viscous response.[23] [24] Including fluctuations together with the cou-plings between shape dynamics, interfacial flow, and curvature described here, may help better understand probe mobility at different scales, and establish a link with molecular dynamics observations and simulations.[43,48]

Acknowledgements

We acknowledge the support of the European Research Council under the European Community's 7th Framework Programme (FP7/2007-2013)/ERC grant agreement nr 240487. MR acknowledges the support of the Spanish Government through grant BES-2008-003274. MA acknowledges the support received through the prize "ICREA Academia" for excellence in research, funded by the Generalitat de Catalunya.

A New form of the viscous dissipation potential for a Newtonian fluid interface

We start from the form of the interfacial viscous dissipation potential in Eq. (3). By defining the tangential component of the rate-of-deformation tensor, $\widehat{d} = (1/2)\left(\nabla_s v + \nabla_s v^T\right) = d + v_n k$, we have

$$d : d = \widehat{d} : \widehat{d} - 2v_n k : \nabla_s v + v_n^2(4H^2 - 2K). \tag{35}$$

Examining the first term, we have

$$\widehat{d} : \widehat{d} = \frac{1}{2}\nabla_s v : \nabla_s v + \frac{1}{2}\nabla_s v : \nabla_s v^T. \tag{36}$$

We now focus on $\nabla_s v : \nabla_s v$. As discussed in[29] and references therein, while the surface Laplacian for a function is unambiguous, there are two different notions of surface Laplacian for a vector field. On the one hand, the rough Laplacian of a vector field v can be computed as $(\hat{\Delta}_s v)^i = g^{jk} v^i{}_{|jk}$, where by $(\cdot)_{|i}$ we denote covariant differentiation. On the other hand, acting on differential 1-forms, e.g. $g_{ij}v^j$, on can define the Laplace-de Rham operator $\Delta_s^R = -\delta d - d\delta$, where d and δ are the exterior derivative and co-differential operator respectively[49,50]. In the language of vector calculus, $\Delta_s^R v = -\nabla_s \times \nabla_s \times v + \nabla_s(\nabla_s \cdot v)$. The two Laplacians are related by the Bochner formula $\hat{\Delta}_s v = \Delta_s^R v + Kv$. With a direct calculation and the Bochner formula, we have

$$\nabla_s v : \nabla_s v = \frac{1}{2}\Delta_s |v|^2 - v \cdot \hat{\Delta}_s v = \frac{1}{2}\Delta_s |v|^2 - v \cdot \Delta_s^R v - K|v|^2. \tag{37}$$

Indeed, recalling that the covariant differentiation of the metric vanishes, we have

$$\begin{aligned} \frac{1}{2}\Delta_s |v|^2 &= \frac{1}{2} g^{kl}(g_{ij} v^i v^j)_{|kl} = g_{ij} g^{kl} (v^i{}_{|k} v^j)_{|l} \\ &= g_{ij} g^{kl} v^i{}_{|kl} v^j + g_{ij} g^{kl} v^i{}_{|k} v^j{}_{|l}. \end{aligned} \tag{38}$$

From standard identities of exterior calculus on manifolds[51], we have the following equations

$$\begin{aligned} v \cdot (\delta dv) &= |dv|^2 - \star d(v \wedge \star dv), \\ v \cdot (d\delta v) &= |\delta v|^2 - \star d(\delta v \wedge \star v), \end{aligned} \tag{39}$$

where $\star$ is the Hodge star operator. Adding these two equations and rewriting in the language of vector calculus, we obtain

$$\begin{aligned}-\boldsymbol{v}\cdot\Delta_s^R\boldsymbol{v} =&|\nabla_s\times\boldsymbol{v}|^2+(\nabla_s\cdot\boldsymbol{v})^2\\ &-\nabla_s\times\left[(\boldsymbol{n}\cdot\nabla_s\times\boldsymbol{v})\boldsymbol{v}-(\nabla_s\cdot\boldsymbol{v})\star\boldsymbol{v}\right],\end{aligned}\tag{40}$$

where $\star\boldsymbol{v}$ is a tangent vector field on Γ orthogonal to $\boldsymbol{v}$. Summarizing the equations above, we obtain

$$\begin{aligned}\nabla_s\boldsymbol{v}:\nabla_s\boldsymbol{v} =& |\nabla_s\times\boldsymbol{v}|^2+(\nabla_s\cdot\boldsymbol{v})^2-K|\boldsymbol{v}|^2\\ &+\frac{1}{2}\Delta_s|\boldsymbol{v}|^2-\nabla_s\times\left[(\boldsymbol{n}\cdot\nabla_s\times\boldsymbol{v})\boldsymbol{v}-(\nabla_s\cdot\boldsymbol{v})\star\boldsymbol{v}\right],\end{aligned}\tag{41}$$

where we point out the important fact that the terms in the second line of this equation are null-Lagrangians, i.e. when integrated over Γ they can be expressed by integration by parts (Stoke's theorem) as an integral over the boundary of Γ. Thus, these terms do not contribute to the Euler-Lagrange equations, and for a closed surface their integral vanishes identically.

We examine now the second term in Eq. (36). Recalling the identity relating the Kronecker delta and the permutation symbol in two dimensions, $\delta_i^j\delta_k^l=\varepsilon_{ik}\varepsilon^{jl}+\delta_i^l\delta_k^j$, we have

$$\begin{aligned}\nabla_s\boldsymbol{v}:\nabla_s\boldsymbol{v}^T &= v^i{}_{|j}v^j{}_{|i}=\delta_i^j\delta_k^l\ v^i{}_{|l}v^k{}_{|j}\\ &=\varepsilon_{ik}\varepsilon^{jl}\ v^i{}_{|l}v^k{}_{|j}+\delta_i^l\delta_k^j\ v^i{}_{|l}v^k{}_{|j}\\ &=\left(\varepsilon_{ik}\varepsilon^{jl}\ v^iv^k{}_{|j}\right)_{|l}-\varepsilon_{ik}\varepsilon^{jl}\ v^iv^k{}_{|jl}+(\nabla_s\cdot\boldsymbol{v})^2.\end{aligned}\tag{42}$$

Manipulating the second term in the last line we find

$$\begin{aligned}\varepsilon_{ik}\varepsilon^{jl}\ v^iv^k{}_{|jl}&=(\delta_i^j\delta_k^l-\delta_i^l\delta_k^j)v^iv^k{}_{|jl}=v^i\left(v^k{}_{|ik}-v^k{}_{|ki}\right)\\ &=K|\boldsymbol{v}|^2,\end{aligned}\tag{43}$$

where in the last equality we have used the fact that the second covariant derivative does not commute. Thus, we obtain

$$\nabla_s\boldsymbol{v}:\nabla_s\boldsymbol{v}^T=(\nabla_s\cdot\boldsymbol{v})^2-K|\boldsymbol{v}|^2+\left(\varepsilon_{ik}\varepsilon^{jl}\ v^iv^k{}_{|j}\right)_{|l},\tag{44}$$

where the last term is a divergence, and therefore a null Lagrangian. Collecting all the terms, we have

$$\widehat{\boldsymbol{d}}:\widehat{\boldsymbol{d}}=\frac{1}{2}|\nabla_s\times\boldsymbol{v}|^2+(\nabla_s\cdot\boldsymbol{v})^2-K|\boldsymbol{v}|^2+\mathscr{N}(\boldsymbol{v}),\tag{45}$$

where $\mathscr{N}(\boldsymbol{v})$ is a null Lagrangian collecting the last two terms in Eq. (41) and the last term in Eq. (44). Integrating $\mathscr{N}(\boldsymbol{v})$ over a surface with boundary, it is easy to find the resulting boundary terms. For a closed surface, we find the form of the dissipation potential in Eq. (4), or recalling local inextensibility the alternative form in Eq. (5). The derivation of the tangential and normal Euler-Lagrange equations (7,8) follows directly by taking variations, integrating by parts, and recalling that $\nabla_s\cdot(\boldsymbol{k}-2H\boldsymbol{g})=0$ due to the Codazzi-Mainardi relations.

B Calculations in vector cylindrical harmonic

Using the vectorial form of cylindrical harmonics for the surface velocity field Eq. (13), it is easy to derive the following identities

$$\begin{aligned}\nabla_s\times\boldsymbol{v}_{nm}&=-\frac{\lambda_{nm}}{r_0}v_{nm}^{(2)}\boldsymbol{Y}_{nm},\qquad \nabla_s\cdot\boldsymbol{v}_{nm}=-\frac{\lambda_{nm}}{r_0}v_{nm}^{(1)}Y_{nm},\\ \nabla_s\boldsymbol{v}_{nm}:\boldsymbol{k}&=-\frac{1}{r_0^2}\left(m^2v_{nm}^{(1)}Y_{nm}-mk_nr_0v_{nm}^{(2)}Y_{nm}\right),\end{aligned}$$

where $\lambda_{nm}=r_0^2k_n^2+m^2$. We also have the orthogonality relations

$$\begin{aligned}\int_\Gamma\boldsymbol{Y}_{nm}^*(\theta,z)\cdot\boldsymbol{Y}_{n'm'}(\theta,z)\,dS &= 2\pi r_0L\delta_{nn'}\delta_{mm'},\\ \int_\Gamma\boldsymbol{\Psi}_{nm}^*(\theta,z)\cdot\boldsymbol{\Psi}_{n'm'}(\theta,z)\,dS &= 2\lambda_{nm}\pi r_0L\delta_{nn'}\delta_{mm'},\\ \int_\Gamma\boldsymbol{\Phi}_{nm}^*(\theta,z)\cdot\boldsymbol{\Phi}_{n'm'}(\theta,z)\,dS &= 2\lambda_{nm}\pi r_0L\delta_{nn'}\delta_{mm'}.\end{aligned}$$

C Elastic energy calculations: cylindrical coordinates

Recalling Eq. (11), lengthy but direct calculations lead to the following expressions[38]

$$\begin{aligned}H^2\,dA=&\frac{1}{4r_0}\left[1-\frac{u}{r_0}+\frac{u^2}{r_0^2}-2r_0\Delta_su+r_0^2\left(\Delta_su\right)^2\right.\\ &\left.-\frac{1}{2}\left(u_{,z}\right)^2+\frac{3}{2r_0^2}\left(u_{,\theta}\right)^2+\frac{4uu_{,\theta\theta}}{r_0^2}\right]d\theta dz,\end{aligned}$$

$$2H\,dA=\left(\frac{u_{,\theta}^2+uu_{,\theta\theta}-r_0u_{,\theta\theta}}{r_0^2}-r_0u_{,zz}-uu_{,zz}+1\right)d\theta dz,$$

$$dA=\frac{1}{2r_0}\left(r_0^2u_{,z}^2+2r_0^2+2ur_0+u_{,\theta}^2\right)d\theta dz,$$

where $\Delta_su=u_{,\theta\theta}+u_{,zz}/r_0^2$.

D Bulk fluid traction: tubular membranes

The components of the matrix that maps the bulk and surface representations of the velocity field are

$$
\begin{aligned}
Q^{\pm}_{11} &= \left[\mp|k_n|r_0 P^{\pm}_{m+1} + mP^{\pm}_m\right]/r_0,\\
Q^{\pm}_{12} &= imP^{\pm}_m/r_0,\\
Q^{\pm}_{13} &= \left[(\lambda_{nm}-m)P^{\pm}_m \pm |k_n|, r_0 P^{\pm}_{m+1}\right]/r_0,\\
Q^{\pm}_{21} &= imP^{\pm}_m/r_0,\\
Q^{\pm}_{22} &= \left[\pm|k_n|r_0 P^{\pm}_{m+1} - mP^{\pm}_m,\right]/r_0,\\
Q^{\pm}_{23} &= i\left[\left(m^2-m\right)P^{\pm}_m \mp m|k_n|r_0 P^{\pm}_{m+1}\right]/r_0,\\
Q^{\pm}_{31} &= ik_n r_0 P^{\pm}_m/r_0,\\
Q^{\pm}_{32} &= 0,\\
Q^{\pm}_{33} &= ik_n\left[(m+1)P^{\pm}_m \mp |k_n|r_0 P^{\pm}_{m+1}\right],
\end{aligned}
$$

where we have dropped the subindices nm. We note that in these expressions $P^{\pm}_m = P^{\pm}_m(K_n r_0)$ are scalars that depend on n and m alone, since the radius is fixed on the cylinder.

In Eq. (26), the nonzero components of $\mathbf{S}^{\pm}_{nm}$ are given by

$$
\begin{aligned}
S^{\pm}_{11} &= 2\left[\pm|k_n|r_0 P^{\pm}_{m+1} + (\lambda_{nm}-m)P^{\pm}_m\right]/r_0^2\\
S^{\pm}_{13} &= 2\left[\mp|k_n|r_0(1+\lambda_{nm})P^{\pm}_{m+1} + (m-1)(\lambda_{nm}-m)P^{\pm}_m\right]/r_0^2\\
S^{\pm}_{22} &= -\left[\pm 2|k_n|r_0 P^{\pm}_{m+1} + \left(\lambda_{nm}+m^2-2m\right)P^{\pm}_m\right]/r_0^2\\
S^{\pm}_{32} &= -k_n m P^{\pm}_m/r_0\\
S^{\pm}_{12} &= 2mi\left[\mp|k_n|r_0 P^{\pm}_{m+1} + (m-1)P^{\pm}_m\right]/r_0^2\\
S^{\pm}_{21} &= 2mi\left[(m-1)P^{\pm}_m \mp |k_n|r_0 P^{\pm}_{m+1}\right]/r_0^2\\
S^{\pm}_{23} &= 2mi\left[(\lambda_{nm}+1-2m)P^{\pm}_m \pm 2|k_n|r_0 P^{\pm}_{m+1}\right]/r_0^2\\
S^{\pm}_{31} &= 2k_n i\left[mP^{\pm}_m \mp |k_n|r_0 P^{\pm}_{m+1}\right]/r_0\\
S^{\pm}_{33} &= 2i\lambda_{nm}k_n P^{\pm}_m/r_0,
\end{aligned}
$$

where we have dropped the subindices nm.

Recalling the final expression for the bulk dissipation matrices, and introducing some notation

$$
\mathbf{D}^{\text{bulk}}_{nm} = 2\pi r_0 L\mu_b\left[\underbrace{-\mathbf{S}^{+}_{nm}\left(\mathbf{Q}^{+}_{nm}\right)^{-1}}_{\mathbf{D}^{+}_{nm}} + \underbrace{\mathbf{S}^{-}_{nm}\left(\mathbf{Q}^{-}_{nm}\right)^{-1}}_{\mathbf{D}^{-}_{nm}}\right]
$$

we have the following expressions for the components of these matrices

$$
\begin{aligned}
D^{+}_{11} &= \frac{-2|k_n|\left(k_n^2r^2 - |k_n|r(3m+2)\alpha_+ + (4m+2m^2-2k_n^2r^2)\alpha_+^2 + 2|k_n|rm\alpha_+^3\right)}{|k_n^3|r^3 - (3k_n^2r^2m+2k_n^2r^2)\alpha_+ + |k_nr|(2m^2+4m-k_n^2r^2)\alpha_+^2 + mk_n^2r^2\alpha_+^3}\\
D^{+}_{12} &= \frac{-2im|k_n|\left(k_n^2r^2 - (2|k_nr|+3|k_nr|m)\alpha_+ + (2m^2+4m-k_n^2r^2)\alpha_+^2 + (1+m)|k_nr|\alpha_+^3\right)}{|k_n^3|r^3 - (3m+2)k_n^2r^2\alpha_+ + (4m+2m^2-k_n^2r^2)r|k_n|\alpha_+^2 + k_n^2r^2m\alpha_+^3}\\
D^{+}_{12} &= -D^{+}_{21}\\
D^{+}_{13} &= \frac{-2i|k_n|k_nr\left(k_n^2r^2 - |k_nr|(3m+1)\alpha_+ + (2m+2m^2-k_n^2r^2)\alpha_+^2 + |k_nr|m\alpha_+^3\right)}{|k_n^3|r^3 - k_n^2r^2(3m-2)\alpha_+ + |k_n|r(2m^2+4m-k_n^2r^2)\alpha_+^2 + k_n^2r^2m\alpha_+^3}\\
D^{+}_{13} &= -D^{\text{bulk}+}_{31}\\
D^{+}_{22} &= \frac{|k_n|\left(-2k_n^2r^2 + |k_nr|(4-k_n^2r^2+6m)\alpha_+ + (4k_n^2r^2-8m-4m^2+2k_n^2r^2m)\alpha_+^2 + (|k_n^3|r^3 - 4|k_n|rm)\alpha_+^3\right)}{|k_n^3|r^3 - k_n^2r^2(3m+2)\alpha_+ + |k_n|r(2m^2+4m-k_n^2r^2)\alpha_+^2 + k_n^2r^2m\alpha_+^3}\\
D^{+}_{23} &= \frac{-m|k_n|k_nr\alpha_+(-|k_nr| + 2m\alpha_+ + \alpha_+^2|k_nr|)}{|k_n^3|r^3 - k_n^2r^2(3m+2)\alpha_+ + |k_nr|(2m^2+4m-k_n^2r^2)\alpha_+^2 + mk_n^2r^2\alpha_+^3}\\
D^{+}_{32} &= D^{+}_{23}\\
D^{+}_{33} &= \frac{|k_n|(2k_n^2r^2 - |k_nr|(6m+m^2)\alpha_+ + (4m^2+2m^3)\alpha_+^2 + |k_nr|m^2\alpha_+^3)}{|k_n^3|r^3 - (2k_n^2r^2+3k_n^2r^2m)\alpha_+ + |k_nr|(2m^2+4m\alpha_+^2-k_n^2r^2)\alpha_+^2 + k_n^2r^2\alpha_+^3m}
\end{aligned}
$$

$$
\begin{aligned}
D_{11}^{-} &= \frac{-2|k_n|\left(-k_n^2r^2-|k_n|r(2+3m)\alpha_- -(2m^2-4m+2k_n^2r^2)\alpha_-^2+2|k_n|rm\alpha_-^3\right)}{-|k_n^3|r^3-k_n^2r^2(3m+2)\alpha_- +|k_n|r(k_n^2r^2-2m^2-4m)\alpha_-^2+k_n^2r^2m\alpha_-^3} \\
D_{12}^{-} &= \frac{-2im|k_n|\left(-k_n^2r^2-|k_n|r(3m+2)\alpha_- -(2m^2+4m+k_n^2r^2)\alpha_-^2+|k_n|r(m+1)\alpha_-^3\right)}{-|k_n^3|r-k_n^2r^2(3m+2)\alpha_- |k_n|r(-2m^2-4m+k_n^2r^2)\alpha_-^2+k_n^2r^2m\alpha_-^3} \\
D_{21}^{-} &= -D_{12}^{-} \\
D_{13}^{-} &= \frac{-2ik_n|k_n|r\left(-k_n^2r^2+(k_n^2r^2-2m-2m^2)\alpha_-^2-|k_n|r(3m+1)\alpha_- +|k_n|rm\alpha_-^3\right)}{-|k_n^3|r^3-k_n^2r^2(3m+2)\alpha_- +|k_n|r(k_n^2r^2-2m^2-4m)\alpha_-^2+k_n^2r^2m\alpha_-^3} \\
D_{31}^{-} &= -D_{13}^{-} \\
D_{22}^{-} &= \frac{|k_n|\left(2k_n^2r^2+|k_n|r(6m+4-k_n^2r^2)\alpha_- +(-2k_n^2r^2m+4m^2+8m-4k_n^2r^2)\alpha_-^2+|k_n|r(k_n^2r^2-4m)\alpha_-^3\right)}{-|k_n^3|r^3-k_n^2r^2(3m+2)\alpha_- +|k_n|r(k_n^2r^2-2m^2-4m)\alpha_-^2+k_n^2r^2m\alpha_-^3} \\
D_{23}^{-} &= \frac{-m\alpha_-k_n|k_n|r\left(-|k_n|r-2m\alpha_- +\alpha_-^2|k_n|r\right)}{-|k_n^3|r^3-k_n^2r^2(3m+2)\alpha_- +|k_n|r(k_n^2r^2-2m^2-4m)\alpha_-^2+k_n^2r^2m\alpha_-^3} \\
D_{32}^{-} &= D_{23}^{-} \\
D_{33}^{-} &= \frac{|k_n|\left(2k_n^2r^2+|k_n|rm(6+m)\alpha_- -|k_n|rm^2\alpha_-^3+(4m^2+2m^3)\alpha_-^2\right)}{|k_n^3|r^3+k_n^2r^2(3m+2)\alpha_- +|k_n|r(2m^2+4m-k_n^2r^2)\alpha_-^2-k_n^2r^2\alpha_-^3m}
\end{aligned}
$$

where we have dropped the subindices nm and $\alpha_\pm = P_m^\pm / P_{m+1}^\pm$.

References

1 H. Sprong, P. van der Sluijs and G. van Meer, *Nat. Rev. Mol. Cell. Bio.*, 2001, **2**, 504–513.
2 U. Seifert, *Advances in Physics*, 1997, **46**, 13–137.
3 I. Tsafrir, Y. Caspi, M. A. Guedeau-Boudeville, T. Arzi and J. Stavans, *Phys. Rev. Lett.*, 2003, **91**, 138102.
4 J. B. Fournier, N. Khalifat, N. Puff and M. I. Angelova, *Phys. Rev. Lett.*, 2009, **102**, 018102.
5 M. Fardin, O. Rossier, P. Rangamani, P. Avigan, N. Gauthier, W. Vonnegut, A. Mathur, J. Hone, R. Iyengar and M. Sheetz, *Soft Matter*, 2010, **6**, 4788–4799.
6 M. Staykova, M. Arroyo, M. Rahimi and H. Stone, *Physical Review Letters*, 2013, **110**, 028101.
7 P. G. Saffman and M. Delbrück, *Proc. Natl. Acad. Sci. U.S.A.*, 1975, **72**, 3111–3113.
8 P. Cicuta, S. L. Keller and S. L. Veatch, *The Journal of Physical Chemistry B*, 2007, **111**, 3328–3331.
9 A. Rustom, R. Saffrich, I. Markovic, P. Walther and H. Gerdes, *Science*, 2004, **303**, 1007–1010.
10 K. Simons and W. Vaz, *Annu. Rev. Biophys. Biomol. Struct.*, 2004, **33**, 269–295.
11 B. M. Discher, Y. Y. Won, D. S. Ege, J. C. M. Lee, F. S. Bates, D. E. Discher and D. A. Hammer, *Science*, 1999, **284**, 1143–1146.
12 R. Dimova, U. Seifert, B. Pouligny, S. Forster and H. Dobereiner, *Eur. Phys. J. E*, 2002, **7**, 241–250.
13 Y. Gambin, R. Lopez-Esparza, M. Reffay, E. Sierecki, N. S. Gov, M. Genest, R. S. Hodges and W. Urbach, *Proceedings of the National Academy of Sciences of the United States of America*, 2006, **103**, 2098–2102.
14 M. Henle and A. Levine, *Physical Review E*, 2010, **81**, 011905.
15 Y. A. Domanov, S. Aimon, G. E. Toombes, M. Renner, F. Quemeneur, A. Triller, M. S. Turner and P. Bassereau, *Proceedings of the National Academy of Sciences*, 2011, **108**, 12605–12610.
16 H. Stone and A. Ajdari, *Journal of Fluid Mechanics*, 1998, **369**, 151–174.
17 A. J. Levine, T. Liverpool and F. C. MacKintosh, *Physical Review Letters*, 2004, **93**, 38102.
18 E. P. Petrov and P. Schwille, *Biophys. J.*, 2008, **94**, L41–L43.
19 B. A. Camley and F. L. H. Brown, *Phys. Rev. E*, 2012, **85**, 061921.
20 R. Dimova, S. Aranda, N. Bezlyepkina, V. Nikolov, K. A. Riske and R. Lipowsky, *J. Phys-Condens. Mat.*, 2006, **18**, S1151–S1176.
21 *Proceedings of the National Academy of Sciences*, 2011, **108**, 14705.
22 U. Seifert and S. A. Langer, S. A., *Europhys. Lett.*, 1993, **23**, 71–76.
23 E. Reister-Gottfried, S. M. Leitenberger and U. Seifert, *Phys. Rev. E*, 2007, **75**, 011908.
24 A. Naji and F. L. H. Brown, *The Journal of Chemical Physics*, 2007, **126**, 235103.
25 J. J. Lin, P. P. Ghoroghchian, Y. Zhang and D. A. Hammer, *Langmuir*, 2006, **22**, 3975–3979.
26 T. O. Pangburn, F. S. Bates and E. Kokkoli, *Soft Matter*, 2012, **8**, 4449–4461.
27 L. Scriven, *Chem. Eng. Sci.*, 1960, **12**, 98–108.
28 T. Secomb and R. Skalak, *Q. J. Mech. Appl. Math.*, 1982, **35**, 233–47.
29 M. Arroyo and A. DeSimone, *Phys. Rev. E*, 2009, **79**, 031915.
30 T. G. Mason and D. Weitz, *Physical review letters*, 1995, **74**, 1250–1253.
31 T. M. Squires and T. G. Mason, *Annual Review of Fluid Mechanics*, 2010, **42**, 413–438.
32 E. Evans and A. Yeung, *Chem. Phys. Lipids*, 1994, **73**, 39–56.
33 M. Rahimi and M. Arroyo, in preparation.
34 M. Rahimi and M. Arroyo, *Physical Review E*, 2012, **86**, 011932.
35 R. Barrera, G. Estevez and J. Giraldo, *European Journal of Physics*, 2000, **6**, 287.
36 G. Dorries and G. Foltin, *Physical Review E*, 1996, **53**, 2547–2550.
37 H. Goldstein, C. Poole and J. Safko, *Classical Mechanics*, Addison-Wesley, 2001.
38 D. Bukman, J. Yao and M. Wortis, *Physical Review E*, 1996, **54**, 5463.

39 J. Happel and H. Brenner, *Low Reynolds number hydrodynamics: with special applications to particulate media*, Springer, 1965, vol. 1.

40 R. Zwanzig and M. Bixon, *Physical Review A*, 1970, **2**, 2005.

41 R. Phillips, J. Kondev, J. Theriot and H. G. Garcia, *Physical biology of the cell*, Garland Science, 2013.

42 N. M. Sherer, *Molecular Biology of the Cell*, 2013, **24**, 1095–1098.

43 S. Busch, C. Smuda, L. C. Pardo and T. Unruh, *Journal of the American Chemical Society*, 2010, **132**, 3232–3233.

44 P. V. Pawar, S. V. Gohil, J. P. Jain and N. Kumar, *Polym. Chem.*, 2013, **4**, 3160–3176.

45 S. Egli, H. Schlaad, N. Bruns and W. Meier, *Polymers*, 2011, **3**, 252–280.

46 A. Naji, A. J. Levine and P. A. Pincus, *Biophys. J.*, 2007, **??**, L49–L51.

47 A. Naji, P. J. Atzberger and F. L. H. Brown, *Phys. Rev. Lett.*, 2009, **102**, 138102.

48 E. Falck, T. Róg, M. Karttunen and I. Vattulainen, *Journal of the American Chemical Society*, 2008, **130**, 44–45.

49 T. Willmore, *Riemannian geometry*, Oxford University Press, 1993.

50 S. Rosenberg, *The Laplacian on a riemannian manifold: an introduction to analysis on manifolds*, Cambridge University Press, 1997.

51 J. Marsden, T. Ratiu and R. Abraham, *Manifolds, tensor analysis and applications*, Springer-Verlag, 1998.